Journal of Medical Ultrasonics (2022) 49:529–543
https://doi.org/10.1007/s10396-022-01229-z

ORIGINAL ARTICLE–PHYSICS & ENGINEERING

Evaluation of local changes in radio-frequency signal waveform and brightness caused by vessel dilatation for ascertaining reliability of elasticity estimation inside heterogeneous plaque: a preliminary study

Yuta Haji[1] · Shohei Mori[2] · Mototaka Arakawa[1,2] · Toshio Yamagishi[3] · Hiroshi Kanai[1,2]

Received: 4 February 2022 / Accepted: 9 May 2022 / Published online: 16 July 2022

Abstract

Purpose To diagnose plaque characteristics, we previously developed an ultrasonic method to estimate the local elastic modulus from the ratio of the pulse pressure to the strain of the arterial wall due to dilatation in systole by transcutaneously measuring the minute thinning in thickness during one cardiac cycle. For plaques, however, some target regions became thicker as the vessel dilates, resulting in false elasticity. Therefore, a method to identify a reliable target for the elastic modulus estimation is indispensable. As a candidate for an identification index of plaques that become thicker during one cardiac cycle, the correlation of the radio-frequency (RF) signals remains high and it is not sufficient to obtain the elasticity. In this study, we thoroughly observed the target with a high correlation but positive strain in the plaque and characterized it by the property of the surrounding area.

Methods For the plaque formed in the right carotid sinus of a patient with hyperlipidemia and the wall of the right common carotid artery of a young healthy male, (1) the correlation value as the similarity between the RF signals, (2) change in brightness obtained from the log-compressed envelope signals, and (3) strain obtained between the time of the R-wave and that of the maximum vessel dilatation were observed to characterize the region in the plaque.

Results In the plaque, it was found that the region with high correlation and positive strain and its surrounding area could be classified into one of the three typical patterns.

Conclusion As a preliminary study, this study provides a clue to assert the reliability of elasticity estimates for a region with high correlation and positive strain in the plaque based on measurable properties.

Keywords Atherosclerosis · Plaque · Carotid artery · Elasticity · Strain

Introduction

One of the main causes of cerebral and myocardial infarctions is the rupture of vulnerable plaques in atherosclerosis [1, 2]. As atherosclerosis progresses, plaques, which consist of lipid components, form on the vessel walls. The flow of the lipid components into the blood following the rupture of the plaque introduces serious illnesses, such as cerebral or myocardial infarctions. Thus, plaques with a high risk of rupture are rich in soft tissues, such as lipids and blood clots, whereas stable plaques with a low risk of rupture consist of hard tissues, such as fibrotic tissues. Therefore, a noninvasive evaluation of the internal tissue characteristics of the plaque helps to diagnose the risk of plaque rupture.

Computed tomography (CT) [3], magnetic resonance imaging (MRI), and intravascular ultrasound (IVUS) [4, 5] are used to diagnose atherosclerosis. However, CT uses X-ray radiation, CT and MRI require large-scale equipment, and IVUS is invasive; therefore, the use for repeatable follow-ups of plaque in clinics is difficult. The main noninvasive diagnostic method for atherosclerosis is the

✉ Shohei Mori
mori@tohoku.ac.jp

1 Graduate School of Biomedical Engineering, Tohoku University, Sendai 980-8579, Japan

2 Graduate School of Engineering, Tohoku University, Sendai 980-8579, Japan

3 Department of Internal Medicine, Tohoku Kosai Hospital, Sendai 980-0803, Japan

measurement of intima-media thickness (IMT) using ultrasound [6]. This method mainly measures the shape of the arterial wall and the size of the plaque; however, it is insufficient to assess the risk of plaque rupture.

One approach to diagnosing the tissue characteristics of the vessel wall is to measure the stiffness or elasticity of the vessel wall. The vascular compliance [7, 8], pulse wave velocity (PWV) [9, 10], stiffness parameters [11, 12], and elasticity measured from the change in the arterial diameter [13] have been used as indices of stiffness. However, these methods measure the spatially averaged stiffness of the entire vessel wall in the measurement target. Plaque comprises soft tissues, such as lipids, and hard tissues, such as fibrotic tissues, and its structure is heterogeneous. To determine the tissue characteristics of the plaque, it is necessary to characterize the local stiffness rather than the spatially averaged properties of the entire vessel wall.

Our group has proposed a method to estimate the two-dimensional distribution of the local elastic modulus of the arterial wall by measuring its regional minute thinning deformation caused under pulse pressure using an ultrasound system with a transcutaneous linear array probe [14–16]. This method enables the evaluation of local characteristics and composition inside the plaque, which has a heterogeneous structure [17–20]. This method was applied to clinical studies of patients with atherosclerosis [21, 22], lifestyle-related diseases [23], obese subjects [24], and patients with type 2 diabetes [25–27].

In this method, the elastic modulus is obtained using the property where the vessel wall becomes slightly thinner with vessel dilatation during one cardiac cycle based on the volume preservation of the wall as follows: using the correlation, the decrease in the thickness, $\Delta h(n)$, between the two points set along an ultrasonic beam in the arterial wall is measured during one cardiac cycle. Then, the maximum change in thickness, $|\Delta h|_{\max}$, of $\Delta h(n)$ caused by the pulse pressure Δp is obtained. By dividing $|\Delta h|_{\max}$ by the original thickness h_0 before the vessel dilatation, the strain ε along the beam direction is obtained by assuming that there are no displacements in the lateral and/or elevational directions. The elastic modulus E_θ along the circumferential direction θ is estimated by dividing the pulse pressure Δp by the strain ε.

For plaque, however, the strain is sometimes measured as positive in a local region, i.e., regional thickening occurs even though the entire vessel is dilated. Lipid components in the plaque deform fluidly during vessel dilatation, i.e., the property of regional mobility. This property may cause minute local displacement in the lateral and/or elevational directions within the plaque. This mobility is related to the progression of atherosclerosis, and plaques with high mobility show the "jellyfish sign," which is a high-risk factor for stroke [28].

If a target within the plaque is mobile, it may move out from the measured cross-sectional plane or another target may enter into the measured cross-sectional plane with vessel dilatation. These movements disturb the correct evaluation of the elasticity E_θ based on the measured maximum change in thickness, $|\Delta h|_{\max}$, along the ultrasonic beam caused by the pulse pressure Δp, and the resultant apparent strain ε may be positive. Thus, the obtained strain ε should be evaluated by some other indexes. One of the possible indexes is the correlation of the RF signals. However, since these movements are minute, i.e., several tenth micrometers, the correlation of the RF signals remains high even if the resultant strain ε is positive.

In this study, to identify the targets where the measured strain ε becomes unreliable, which is not appropriate for the calculation of the elastic modulus E_θ, we thoroughly observed the local change in RF signals using correlation R and the local change in brightness, ΔB, inside the plaque during vessel dilatation, where the brightness is obtained from the log-compressed enveloped RF signal to widen the dynamic range. These evaluations of R and ΔB were obtained from the time of the R-wave of the electrocardiogram (ECG), just before the beginning of the vessel dilatation, to the time of maximum vessel dilatation. The strain ε, correlation R, and change in brightness ΔB between these two times were observed for each target for plaques, and these were compared with ε, R, and ΔB for the healthy common carotid artery (CCA).

Principles and methods

Measurement of local change in thickness and strain

Let us consider a small target $\left[d_0 - \frac{w}{2}, d_0 + \frac{w}{2}\right]$ around the depth d_0 with width w along the ultrasonic beam in the arterial posterior wall at a time of the R-wave of ECG, as shown in Fig. 1(1). As shown in Fig. 1(2), due to vessel dilatation, the target moves deeper from d_0 to d_n at the nth frame and the target becomes thinner. Let us define the 0th frame by the time of the R-wave of ECG, which is just before the beginning of the vessel dilatation.

Let us describe its thickness at the nth frame by $h_{d_0}(n)$. The thickness at a time of R-wave (0th frame) is set by w (385 μm in this study), i.e., $h_{d_0}(0) = w$, and the local axial displacements of both edges of the target region $\left[d_0 - \frac{w}{2}, d_0 + \frac{w}{2}\right]$ are tracked using RF data. As shown in Fig. 1(2), let us denote these displaced depths by $z_{d_0-\frac{w}{2}}(n) + \left(d_0 - \frac{w}{2}\right)$ and $z_{d_0+\frac{w}{2}}(n) + \left(d_0 + \frac{w}{2}\right)$, where the second terms $\left(d_0 - \frac{w}{2}\right)$ and $\left(d_0 + \frac{w}{2}\right)$ show the initial depths at the 0th frame, where $z_{d_0-\frac{w}{2}}(0) = z_{d_0+\frac{w}{2}}(0) \equiv 0$. The thick-

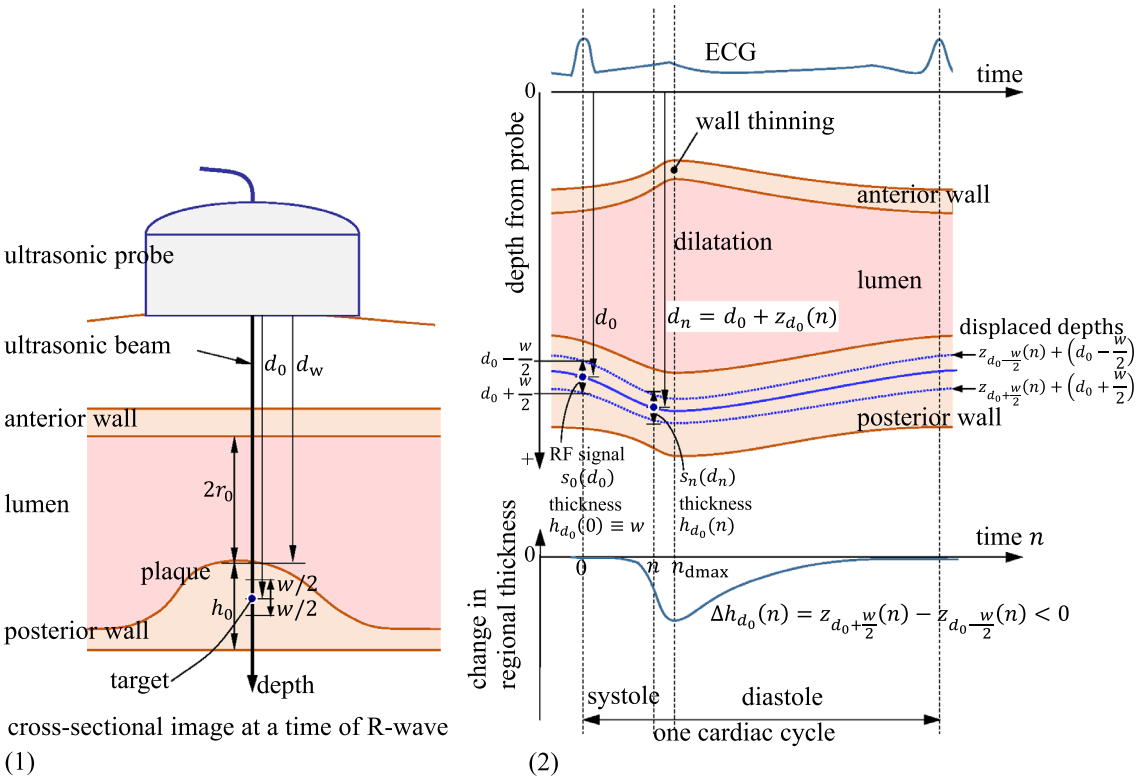

Fig. 1 **(1)** An illustration of a B-mode image around a plaque in the vessel wall and a target at the center depth d_0 with width w along the ultrasonic beam inside the wall at a time of R-wave (0th frame). **(2)** The vessel wall dilates and the wall becomes thin during one cardiac cycle. **a** B-mode image of the CCA of a healthy subject and the analyzed region between the two red lines, and beam position for analysis (white line). Along with the lateral position, **b** correlation $R_{n_{\mathrm{dmax}}}(d_0)$ between RF signals at a time of R-wave and that of the maximum dilatation, **c** strain $\varepsilon(d_0)$ at a time of the maximum dilatation of the vessel. For these data along with 47 lateral positions, **d** distribution of correlation $\{R_{n_{\mathrm{dmax}}}(d_0)\}$ and brightness $\{B_0(d_0)\}$, and **e** distribution of $\{R_{n_{\mathrm{dmax}}}(d_0)\}$ and strain $\{\varepsilon(d_0)\}$. During one cardiac cycle for the data along the white line of **a**, **f** ECG, **g** correlation $R_n(d_0)$ between RF signals at the time of R-wave and that at the nth frame, **h** displacement in the beam direction, $z_{d_0}(n)$, **i** change in thickness, $\Delta h_{d_0}(n)$, and **j** displacement in the lateral direction, $x(n)$

ness $h_{d_0}(n)$ of the target region at the nth frame is obtained by the difference between these displaced depths as

$$h_{d_0}(n) = \left\{ z_{d_0+\frac{w}{2}}(n) + \left(d_0 + \frac{w}{2}\right) \right\} - \left\{ z_{d_0-\frac{w}{2}}(n) + \left(d_0 - \frac{w}{2}\right) \right\}$$
$$= z_{d_0+\frac{w}{2}}(n) - z_{d_0-\frac{w}{2}}(n) + w, [\mathrm{m}] \tag{1}$$

where these displacements, $z_{d_0-\frac{w}{2}}(n)$ and $z_{d_0+\frac{w}{2}}(n)$ are measured using the phased tracking method [29]. Moreover, the change in thickness, $\Delta h_{d_0}(n)$, of the target region is given by

$$\Delta h_{d_0}(n) = h_{d_0}(n) - w$$
$$= z_{d_0+\frac{w}{2}}(n) - z_{d_0-\frac{w}{2}}(n).[\mathrm{m}] \tag{2}$$

As shown in Fig. 1(2), let n_{dmax} be the frame of the time of maximum vessel dilatation, and let us assume that each target in the vessel wall along the ultrasonic beam has the minimum thickness at the n_{dmax}-th frame. The maximum strain $\varepsilon(d_0)$ caused during one cardiac cycle around the target depth d_0 is obtained by

$$\varepsilon(d_0) = \frac{\Delta h_{d_0}(n_{\mathrm{dmax}})}{w} = \frac{z_{d_0+\frac{w}{2}}(n_{\mathrm{dmax}}) - z_{d_0-\frac{w}{2}}(n_{\mathrm{dmax}})}{w}. \tag{3}$$

Calculation of local elasticity of arterial wall

The local elastic modulus $E_\theta(d_0)$ in the circumferential direction for the target set around the center depth d_0 with width w along the ultrasonic beam inside the wall is obtained as follows from the ratio of the pulse pressure Δp measured with a sphygmomanometer to the strain $\varepsilon(d_0)$ measured around the depth d. The derivation of the following equation and the underlying assumptions are described in Appendix:

$$E_\theta(d_0) = \frac{3}{4}\left(\frac{1}{2} + \frac{r_0 + d_0 - \frac{w}{2} - d_{\mathrm{w}}}{w}\right) \frac{\frac{w}{h_0}\Delta p}{-\varepsilon(d_0)}, [\mathrm{Pa}] \tag{4}$$

where $h_0 \geq w$ is the initial thickness of the vessel wall at the time of R-wave, r_0 is the initial inner radius of the vessel at the time of R-wave, and $d_{\mathrm{w}} < d_0$ is the depth of the interface

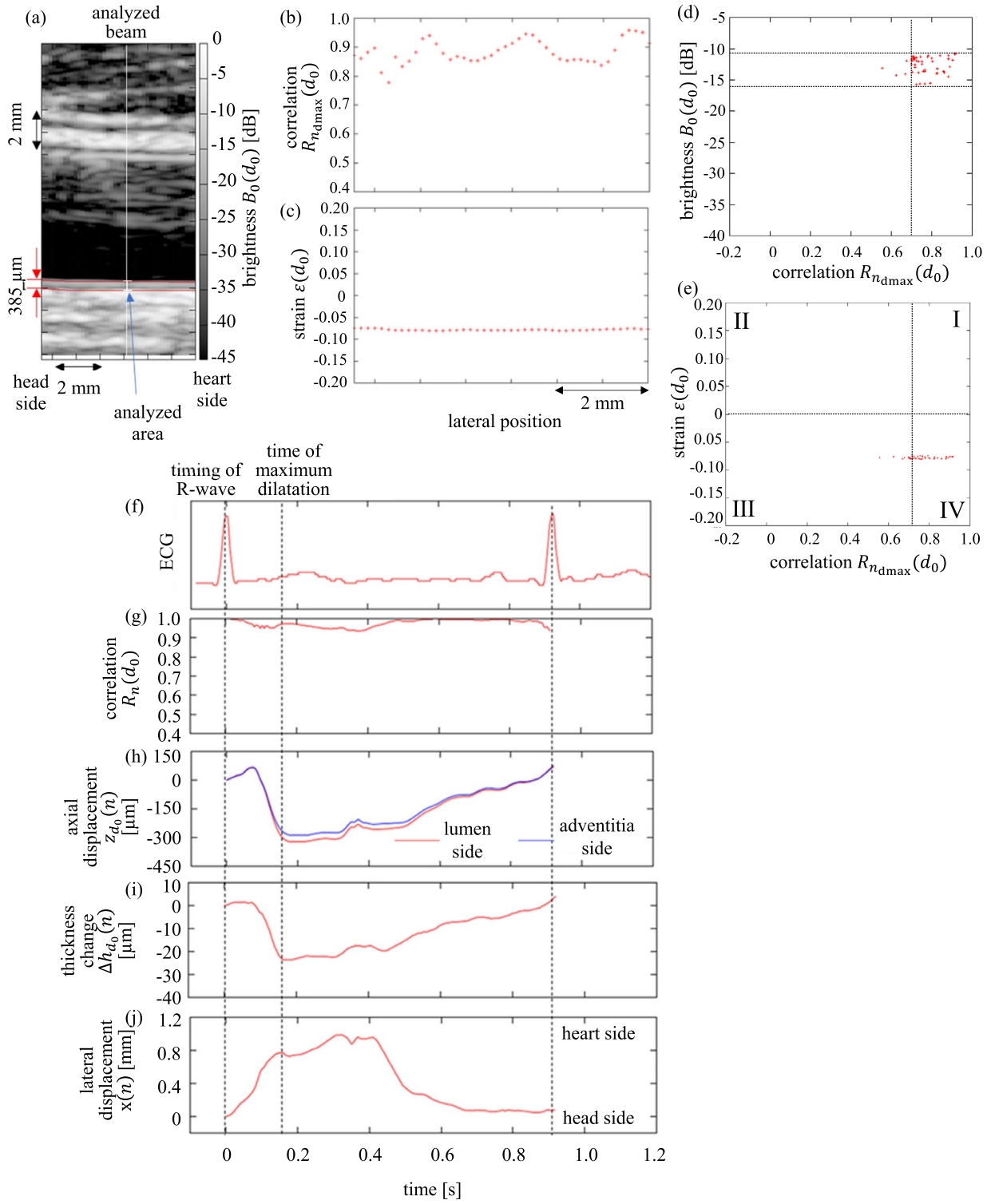

Fig. 1 (continued)

between the lumen and the inner surface of the vessel wall [15, 30, 31], as shown in Fig. 1(1). From this definition, the strain $\varepsilon(d_0)$ should be negative to obtain the elastic modulus $E_\theta(d_0)$.

Evaluation of local change in RF signal waveform due to vessel dilatation

For each frame, an RF signal is acquired along each ultrasonic beam. As shown in Fig. 1(1), let us denote $s_n(d_n)$ as the RF signal of the nth frame around the object, the depth of which is d_n at the nth frame.

The local change in the RF signal with vessel dilatation is evaluated using the normalized cross-correlation $R_n(d_0)$ between the local RF signal $s_0(d_0)$ at the 0th frame and the local RF signal $s_n(d_n)$ at the nth frame. To obtain the $R_n(d_0)$ between local waveforms in the same target inside the plaque, the center position d_n of the correlation window at the nth frame should be maintained at the same position in the depth direction inside the plaque at the 0th frame. This is realized by moving the correlation window with d_n along with the local displaced depth $z_{d_0}(n) + d_0$ for the point set at a depth d_0 of the 0th frame, which is measured by the phased tracking method [29], where $d_n = z_{d_0}(n) + d_0$. Thus, the normalized cross-correlation $R_n(d_0)$ between $s_0(d_0)$ and $s_n(d_n)$ is given by

$$R_n(d_0) = \frac{1}{\sigma_0 \sigma_n} \frac{1}{2N+1} \sum_{i=-N}^{N} \{s_0(d_0 + i \cdot \delta_z) - \overline{s_0}\}\{s_n(d_n + i \cdot \delta_z) - \overline{s_n}\}, \tag{5}$$

where the width of the correlation window is $(2N + 1)$ points, $\overline{s_n}$ and σ_n are the mean and standard deviation of $s_n(d_n)$ in the correlation window at the nth frame, respectively, and δ_z [m] is the spatial interval for sampling the RF signal in the depth direction z, where $\delta_z = 19.25$ μm in this paper. The value of N is determined so that the width of $(2N + 1)$ points $\times \delta_z$ equals $w = 385$ μm.

To deal with $\left|z_{d_0}(n)\right|$ of minute displacement much less than δ_z, the correlation $R_n(d_0)$ of Eq. (5) was interpolated at the sampling interval by a factor M based on the reconstructed interpolation method [32] by convoluting the sinc function. For the lateral direction, the sampling interval was equal to the beam interval δ_x determined by the ultrasonic probe. When the lateral and/or elevational displacements regionally occur in the internal tissues of the plaque due to vessel dilatation, the RF signal may change, and then $R_n(d_0)$ decreases; that is, the high correlation indicates the absence of the effects due to the lateral and/or elevational displacements.

For the actual data, however, some targets become thick even when the vessel wall is dilated, as shown below. Thus, "the correlation being high" is not sufficient to exclude these targets from the calculation of the elastic modulus.

Evaluation of local change in brightness due to vessel dilatation

When local displacements in the lateral and/or elevational directions occur inside the plaque, the brightness values and regional brightness patterns on the B-mode image may change. Therefore, for the same target around the depth d_0 set at the 0th frame along an ultrasonic beam inside the plaque, the change $\Delta B_n(d_0)$ in brightness from the 0th frame to the nth frame is given by

$$\Delta B_n(d_0) = \frac{1}{2N+1} \sum_{i=-N}^{N} \left| B_n(d_n + i \cdot \delta_z) - B_0(d_0 + i \cdot \delta_z) \right|, \text{ [dB]} \tag{6}$$

where $B_n(d)$ [dB] is the brightness with a value of the log-compressed enveloped signal at depth d of the n th frame to increase the dynamic range.

In addition to the strain $\varepsilon(d_0)$ of Eq. (3), the correlation $R_n(d_0)$ of Eq. (5) and the change in brightness $\Delta B_n(d_0)$ of Eq. (6) were evaluated between the time of the R-wave and the time n_{dmax} of the maximum vessel dilatation, i.e., $\varepsilon(d_0)$, $R_{n_{\mathrm{dmax}}}(d_0)$, and $\Delta B_{n_{\mathrm{dmax}}}(d_0)$ were evaluated below.

Measurement of lateral displacement $x(n)$

During one cardiac cycle, lateral displacement of the carotid artery occurs because of the force exerted by contraction of the heart. To detect the effect of lateral displacement on the strain measurement, the lateral displacement $x(n)$ of the entire vessel wall was measured using the block matching method [33, 34], by neglecting the regional difference in the lateral displacement. For calculating the two-dimensional (2D) normalized cross-correlation function of the enveloped RF signals, the size of the region $\mathcal{R}$ was ±0.54 mm in the depth direction by ±1.05 mm in the lateral direction for the plaque and ±0.08 mm in the depth direction by ±1.05 mm in the lateral direction for the CCA. Since the width of the 47 ultrasonic beams in the lateral direction was employed for obtaining $\varepsilon(d_0)$, $R_{n_{\mathrm{dmax}}}(d_0)$, and $\Delta B_{n_{\mathrm{dmax}}}(d_0)$, the region $\mathcal{R}$ was set almost in the center of the lateral direction with 47 beams at the 0th frame. The RF signal contains the amplitude and phase components. Even if an object moves along the lateral direction by keeping its depth, the phase values of the RF signals between the different beam positions randomly change because there is variance in the speed of sound for the soft tissue from the ultrasonic probe to the anterior wall. Thus, the 2D normalized cross-correlation function is obtained from the enveloped RF signal to ignore the phase component.

The employed maximum lag (τ_z, τ_x) in calculating the 2D normalized cross-correlation function was ±0.075 mm in the depth direction and ±0.75 mm in the lateral direction for the plaque and ±0.055 mm in the depth and ±0.75 mm in the lateral direction for the CCA. The data used for the calculation of the cross-correlation function were restricted in the intima-media complex (IMC) for the healthy CCA or inside the plaque. The resultant 2D cross-correlation function is interpolated using a reconstructive interpolation method [32].

Experimental method

A linear array probe with a center frequency of 7.5 MHz and 192 elements was connected to a diagnostic ultrasound system (SSD-6500; Aloka, Japan). The focus was fixed at 18.7 mm from the probe. The sampling frequency of the RF signal was 40 MHz, i.e., the spatial interval δ_z of the signal was 19.25 μm by assuming the speed of sound c_0 to be 1,540 m/s, the frame rate was 286 Hz, and the beam interval δ_x was 150 μm. The width $(2N + 1)$ points for obtaining the correlation in Eq. (5) was set to 21 points, i.e., the actual width w was 385 μm. The factor M in the interpolation of $R_n(d_0)$ of Eq. (5) was set to 10.

The plaque formed in the right carotid sinus of a patient with dyslipidemia in his 50s was measured three times (in March 2012, December 2012, and March 2013). The target region with width w was set in the plaque at every δ_z, and the number of the target regions set along the ultrasonic beam depended on the thickness of the wall. The minimum to maximum numbers of the target regions set along the ultrasonic beam distributed along the lateral direction were 47–96, 30–91, and 66–104 for the respective three measurements. For comparison, the right CCA of a healthy male in his 20s was also measured.

The study protocol was approved by the ethics committee of the Graduate School of Engineering, Tohoku University (19A-5), and the participants agreed to participate in this study.

Results and discussion

Results for the healthy CCA

Figure 1a shows the analyzed region set between the two red lines of the posterior wall on the B-mode image of the CCA of a healthy subject. Since the thickness of the IMC of the healthy subject was thin (385 μm), the number of targets $\{d_0\}$ along the ultrasonic beam for the evaluation of the strain of Eq. (3) and elasticity of Eq. (4) was set to be one. Along the lateral direction for the IMC, 47 targets were set. Figure 1b and c shows the distribution of their correlation $R_{n_{\mathrm{dmax}}}(d_0)$ of Eq. (5) and strain $\varepsilon(d_0)$ of Eq. (3), respectively. Figure 1d shows the relationship between $\{R_{n_{\mathrm{dmax}}}(d_0)\}$ and brightness $\{B_0(d_0)\}$ at the time of the R-wave for 47 targets. Figure 1e shows the relationship between $\{R_{n_{\mathrm{dmax}}}(d_0)\}$ and $\{\varepsilon(d_0)\}$.

Figure 1f–j shows the waveforms obtained during one cardiac cycle in the IMC along the ultrasound beam shown by the white line in Fig. 1a. Figure 1f shows the ECG, Fig. 1g shows the correlation $R_n(d_0)$ of Eq. (5), Fig. 1h shows the axial displacements $z_{d_0-\frac{w}{2}}(n)$ and $z_{d_0+\frac{w}{2}}(n)$ at the lumen and adventitia sides of the vessel wall, respectively; Fig. 1i shows the change $\Delta h_{d_0}(n)$ in thickness of Eq. (2) from the time of the R-wave, and Fig. 1j shows the lateral displacement $x(n)$ from the time of the R-wave.

For the CCA of the healthy subject, the correlation $R_{n_{\mathrm{dmax}}}(d_0)$ of Fig. 1b was higher than 0.7 for all the lateral positions, strain $\varepsilon(d_0)$ of Fig. 1c was almost constant at approximately –0.07, and brightness values $B_0(d_0)$ of Fig. 1d ranged from –16 to –10 dB. As shown in Fig. 1g, the correlation $R_n(d_0)$ was always maintained at high values during one cardiac cycle. As shown in Fig. 1i, the change in the wall thickness,$\Delta h_{d_0}(n)$, became approximately −25 μm with vessel dilatation and then returned to the original zero. As shown in Fig. 1j, the maximum displacement of the CCA in the lateral direction was approximately 1 mm for the heart side.

The waveforms for the change in thickness, $\Delta h_{d_0}(n)$, of Fig. 1i, $R_n(d_0)$ of Fig. 1g, and the lateral displacement $x(n)$ of Fig. 1j were obtained during one cardiac cycle for all ultrasound beams. From these results, the CCA became homogeneously thinner with dilatation and then returned to the original level, the correlation was high, and CCA homogeneously moved in the lateral direction to the heart side in systole. Therefore, the strain $\varepsilon(d_0)$ in Fig. 1c and the elastic modulus $E_\theta(d_0)$ of Eq. (4) were reliable for the CCA of the healthy subject, and $E_\theta(d_0) = 673$ kPa and the correlation $R_n(d_0)$ of Fig. 1g did not decrease, although there was a lateral displacement of about 1 mm.

Results for the plaque for the patient

For the RF data measured in March 2013 for the patient, Fig. 2a shows the analyzed region set between the two red lines on the B-mode image of the plaque of the carotid sinus. In this region, 4115 targets were set, and the analysis described above was applied for each target. Figure 2b shows the distribution of the correlation $\{R_{n_{\mathrm{dmax}}}(d_0)\}$ and the brightness $\{B_0(d_0)\}$ at the time of the R-wave (0th frame). $\{B_0(d_0)\}$ in Fig. 2b ranged more widely than that for the healthy CCA in Fig. 1d. This is because the brightness tends

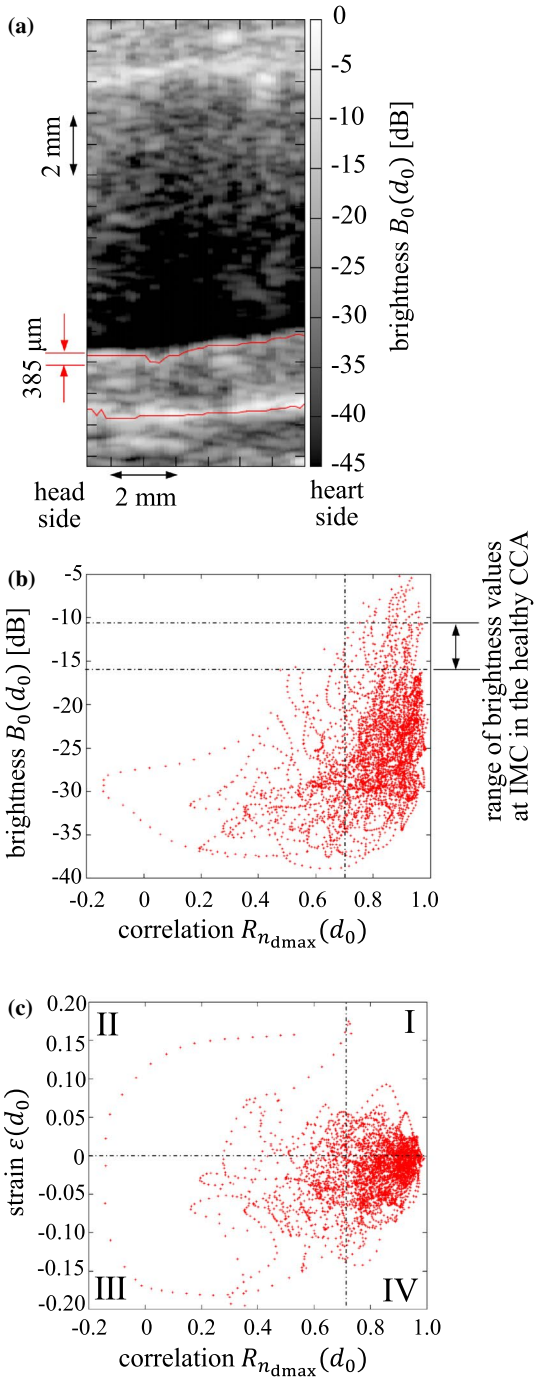

Fig. 2 **a** B-mode image of a plaque at the carotid sinus of a patient and analyzed region between the two red lines. For 4115 targets in the analyzed region, **b** distribution of correlation $\{R_{n_{\mathrm{dmax}}}(d_0)\}$ and brightness $\{B_0(d_0)\}$, and **c** distribution of $\{R_{n_{\mathrm{dmax}}}(d_0)\}$ and strain $\{\varepsilon(d_0)\}$

to be higher for the interface between harder tissues and softer tissues, and the plaque has both soft and hard tissues, which corresponds to the already known fact that the plaque has a heterogeneous structure.

Figure 2c shows the distribution $\{R_{n_{\mathrm{dmax}}}(d_0)\}$ and strain $\{\varepsilon(d_0)\}$ for 4115 targets. There were targets in areas II and III with a low correlation $R_{n_{\mathrm{dmax}}}(d_0)$ and in areas I and II with positive strain $\varepsilon(d_0)$ for the plaque, whereas the target was not observed in these areas I–III for the healthy CCA in Fig. 1e.

For the same data, Fig. 3a and b shows the cross-section images of the correlation $\{R_{n_{\mathrm{dmax}}}(d_0)\}$ and strain $\{\varepsilon(d_0)\}$, respectively. By comparing these images, targets (red or yellow) with positive strain in Fig. 3b have not only a small correlation (blue or green) but also a high correlation (red or orange) in Fig. 3a.

Along the same ultrasonic beam, two targets A and B set in Fig. 3a and b were analyzed in detail as follows, where $d_{0\mathrm{A}}$ and $d_{0\mathrm{B}}$ are the center depths in A and B, respectively. For A, $R_{n_{\mathrm{dmax}}}(d_{0\mathrm{A}}) = 0.94$ and $\varepsilon(d_{0\mathrm{A}}) > 0$, and for B, $R_{n_{\mathrm{dmax}}}(d_{0\mathrm{B}}) = 0.84$ and $\varepsilon(d_{0\mathrm{B}}) < 0$. Figure 3c and d shows the RF signals for targets A and B at the time (0th frame) of the R-wave and at the time (n_{dmax}-th frame) of the maximum dilatation, respectively. The correlation was high for both targets.

Figure 3e–j shows the detailed results (waveforms) for targets A and B during one cardiac cycle. Figure 3e shows the ECG, and Fig. 3f shows $R_n(d_0)$ during one cardiac cycle in each target. Figure 3g and h shows the measured axial displacements $z_{d_{0\mathrm{A}}}(n)$ and $z_{d_{0\mathrm{B}}}(n)$, Fig. 3i shows the changes in thickness $\Delta h_{d_{0\mathrm{A}}}(n)$ and $\Delta h_{d_{0\mathrm{B}}}(n)$, and Fig. 3j shows the measured lateral displacement $x(n)$ of the entire vessel wall. For target A, $R_{n_{\mathrm{dmax}}}(d_{0\mathrm{A}})$ of Fig. 3f remained high and $\Delta h_{d_{0\mathrm{A}}}(n)$ of Fig. 3i returned to the original level after one cardiac cycle, but $\varepsilon(d_{0\mathrm{A}}) > 0$. Thus, for A, the change in thickness is unsuitable for estimation of the elastic modulus $E_\theta(d_0)$ using Eq. (4).

Alternatively, for B, $R_{n_{\mathrm{dmax}}}(d_{0\mathrm{B}}) = 0.84$ was high, and $\Delta h_{d_{0\mathrm{B}}}(n)$ of Fig. 3i became approximately 15 μm thinner and returned to its original value at the time of the succeeding R-wave. As shown in Fig. 3j, the maximum displacement of the vessel in the lateral direction was 109 μm, which is smaller than the beam spacing of 150 μm. If the lateral displacement affects the RF signal for the plaque, the correlation may decrease. However, for both targets A and B, $R_{n_{\mathrm{dmax}}}(d_0)$ remained large during one cardiac cycle, but changes in thickness, $\Delta h_{d_{0\mathrm{A}}}(n_{\mathrm{dmax}})$ and $\Delta h_{d_{0\mathrm{B}}}(n_{\mathrm{dmax}})$, were completely different even though A and B were on the same beam.

Therefore, the displacement of the plaque in the lateral direction caused by vessel dilatation and/or heart contraction does not have a critical influence on the change in the RF signal, and other factors may decrease the correlation. The plaque in Figs. 2 and 3 included targets where the correlation

$R_{n_{\mathrm{dmax}}}(d_0)$ was high but the strain $\varepsilon(d_0)$ was positive. These targets are not suitable for measuring the elastic modulus. However, it is not possible to identify these targets only from the correlation values.

Typical patterns for regions with positive strain despite high correlation in RF signals

As shown in target A in Fig. 3, in the plaque, there were some targets where the strain $\varepsilon(d_0)$ was positive at the time of maximum dilatation, while the high correlation $R_n(d_0)$ was maintained during one cardiac cycle. For such targets, let us observe the change in brightness, $\Delta B_{n_{\mathrm{dmax}}}(d_0)$, of Eq. (6) from the time of the R-wave to the time n_{dmax} at the maximum dilatation as follows:

In Fig. 4a, for the same data as Figs. 2 and 3, the targets with low correlation ($R_{n_{\mathrm{dmax}}}(d_0) < 0.7$) were excluded from the detailed analysis and filled with gray; for the remaining targets, the targets with positive strain ($\varepsilon(d_0) > 0$) and high correlation ($R_{n_{\mathrm{dmax}}}(d_0) \geq 0.7$) and their surroundings were set as regions $\mathbf{R}_1$–$\mathbf{R}_5$ with red frames. The expanded figure for each of $\mathbf{R}_1$–$\mathbf{R}_5$ is shown in Fig. 4(1-a)–(5-a), where the sub-regions with high correlation ($R_{n_{\mathrm{dmax}}}(d_0) \geq 0.7$) but positive strain ($\varepsilon(d_0) > 0$) are surrounded by a black dashed line.

Figure 4b shows the brightness change $\Delta B_{n_{\mathrm{dmax}}}(d_0)$ from the time of the R-wave to the time of maximum vessel dilatation for the same set of regions $\mathbf{R_1}$–$\mathbf{R_5}$. Similar to Fig. 4(1-a)–(5-a), Fig. 4(1-b)–(5-b) shows the expanded figure for each of $\mathbf{R_1}$–$\mathbf{R_5}$ in Fig. 4b for $\Delta B_{n_{\mathrm{dmax}}}(d_0)$.

Figures 5 and 6 show the analyzed results for the second and third data from the carotid sinus of the same subject measured on two different days, respectively (December 2012 for Fig. 6, and March 2013 for Fig. 5). Figure 5a and b shows the distributions of strain $\varepsilon(d_0)$ and brightness changes $\Delta B_{n_{\mathrm{dmax}}}(d_0)$ for the second data, and Fig. 6a and b shows their distributions for the third data. For these images, as shown in Fig. 4, after excluding targets with low

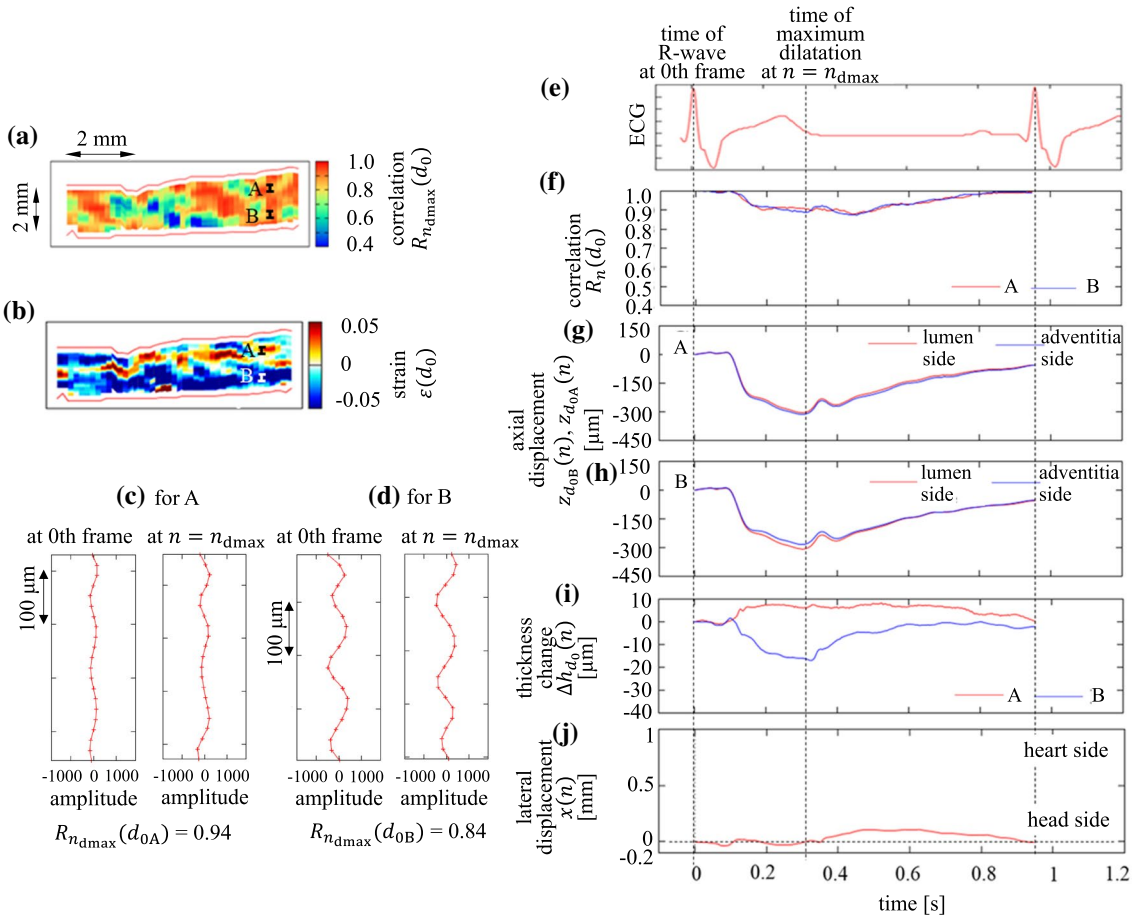

Fig. 3 For the same data of the arterial wall in Fig. 2, the cross-sectional images of **a** correlation $R_{n_{\mathrm{dmax}}}(d_0)$ and **b** strain $\varepsilon(d_0)$. **c**, **d** RF signals for targets A and B at the time of R-wave and at the time of the maximum dilatation, respectively. For targets A and B set in **a** and **b**, the waveforms of **e** the ECG, **f** the correlation $R_n(d_0)$, **g, h** the measured axial displacements $z_{d_0}(n)$, **i** the changes in thickness, $\Delta h_{d_0}(n)$, and **j** the measured lateral displacement $x(n)$ of the entire region during one cardiac cycle

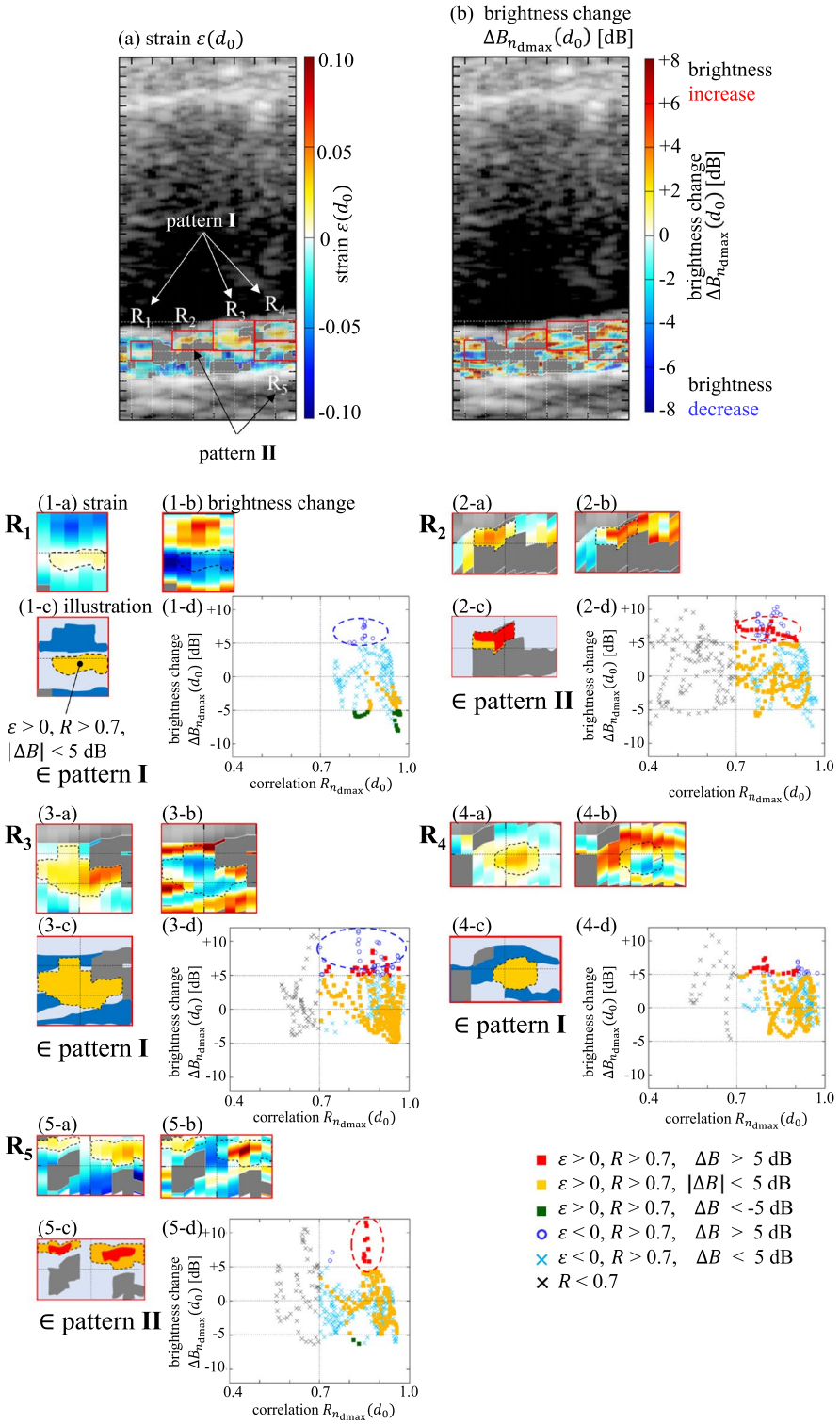

Fig. 4 The cross-sectional images of **a** strain $\varepsilon(d_0)$ and **b** change in brightness, $\Delta B_{n_{\mathrm{dmax}}}(d_0)$, for the target regions of high correlation ($R_{n_{\mathrm{dmax}}}(d_0) \geqq 0.7$) of RF signals on the cross-sectional image of the plaque. The targets with low correlation ($R_{n_{\mathrm{dmax}}}(d_0) < 0.7$) are filled with gray. Five regions $\mathbf{R_1}$–$\mathbf{R_5}$ where strains $\varepsilon(d_0)$ are positive are denoted by the red frames. For each of the regions $\mathbf{R_1}$ to $\mathbf{R_5}$, **(1)**–**(5)** show **a** the magnified cross-sectional images of the distribution of the strains $\{\varepsilon(d_0)\}$, **b** the magnified images of the distribution of changes in brightness, $\{\Delta B_{n_{\mathrm{dmax}}}(d_0)\}$, **c** an illustration for explanation, and **d** distribution of correlation $\{R_{n_{\mathrm{dmax}}}(d_0)\}$ and $\{\Delta B_{n_{\mathrm{dmax}}}(d_0)\}$ for targets in each region. In **c** and **d**, the color of each plotted point is distinguished by the values of $\varepsilon(d_0)$, $R_{n_{\mathrm{dmax}}}(d_0)$, and $\Delta B_{n_{\mathrm{dmax}}}(d_0)$

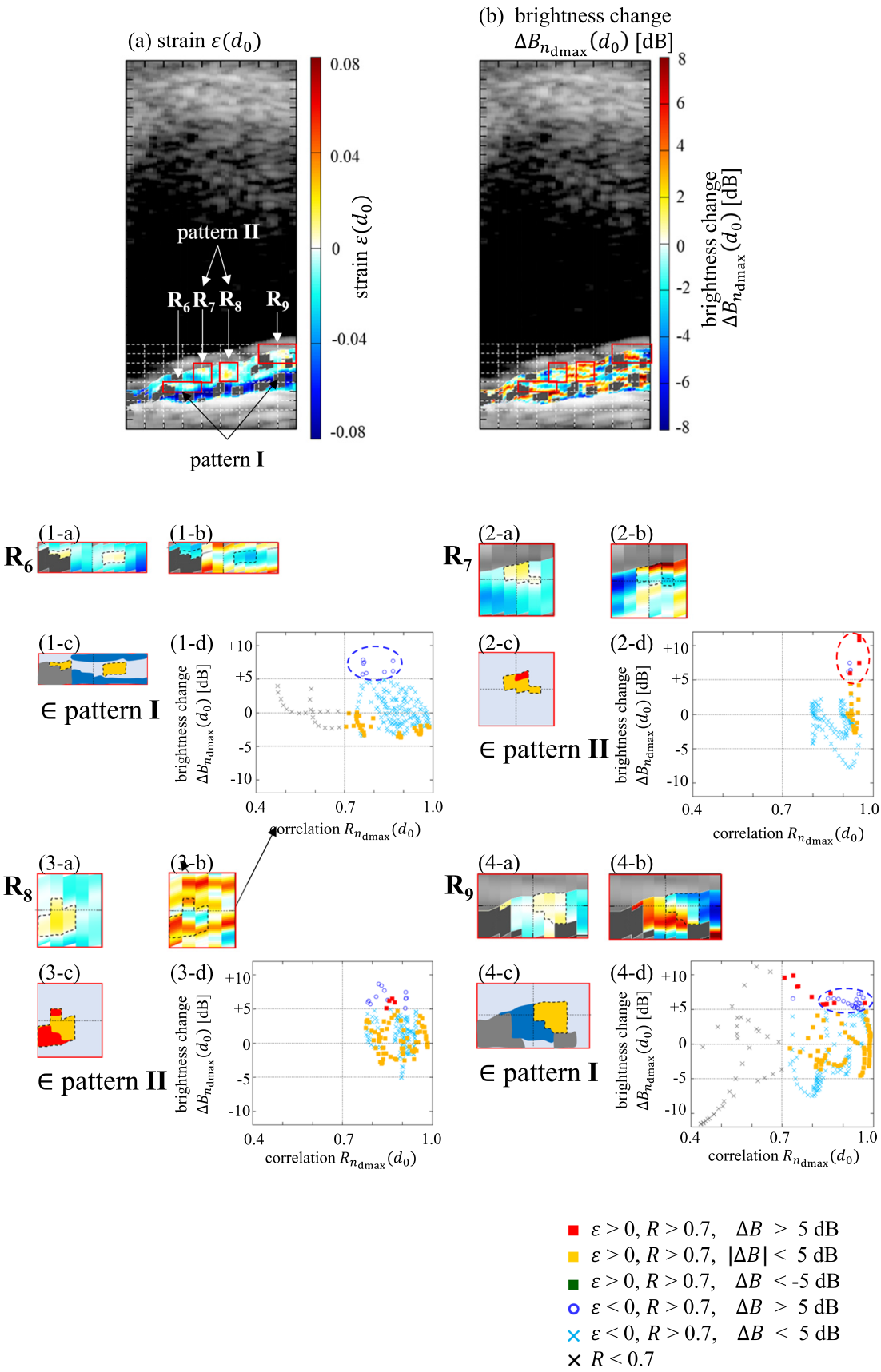

Fig. 5 For the second data from the carotid sinus of the same subject, **a**, **b** (**1**)–(**4**) are shown in a format similar to Fig. 4. In **a** and **b**, four regions $\mathbf{R_6}$–$\mathbf{R_9}$ where strains $\varepsilon(d_0)$ are positive are denoted by the red frames

correlation ($R_{n_{\mathrm{dmax}}}(d_0) < 0.7$), for the remaining targets, the targets with high correlation ($R_{n_{\mathrm{dmax}}}(d_0) \geqq 0.7$) and positive strain ($\varepsilon(d_0) > 0$) and their surroundings are defined as four regions $\mathbf{R_6}$–$\mathbf{R_9}$ for Fig. 5a and b, and five regions $\mathbf{R_{10}}$–$\mathbf{R_{14}}$ for Fig. 6a and b.

From the observations using regional strain $\varepsilon(d_0)$ of Eq. (3), the correlation $R_{n_{\mathrm{dmax}}}(d_0)$ of Eq. (5), and the brightness change $\Delta B_{n_{\mathrm{dmax}}}(d_0)$ of Eq. (6), we found that all of the 14 regions ($\mathbf{R_1}$–$\mathbf{R_{14}}$) with high correlation but positive strain and their surroundings in Figs. 4, 5, and 6 were classified into one of the following three characteristic patterns **I**—**III**, as illustrated in Fig. 7a–c.

For Pattern **I**, the sub-region (yellow) with high correlation and $\left|\Delta B_{n_{\mathrm{dmax}}}(d_0)\right| < 5$ dB but positive strain ($\varepsilon(d_0) > 0$) at the center is surrounded by the sub-region (blue) where the brightness increases ($\Delta B_{n_{\mathrm{dmax}}}(d_0) > 5$ dB) with negative strain ($\varepsilon(d_0) < 0$). For Pattern **II**, inside the sub-region (yellow) with high correlation and $\left|\Delta B_{n_{\mathrm{dmax}}}(d_0)\right| < 5$ dB but positive strain ($\varepsilon(d_0) > 0$), there is a sub-region (red) where the brightness increases ($\Delta B_{n_{\mathrm{dmax}}}(d_0) > 5$ dB) with positive strain. For Pattern **III**, inside the sub-region (yellow) with high correlation and $\left|\Delta B_{n_{\mathrm{dmax}}}(d_0)\right| < 5$ dB but positive strain ($\varepsilon(d_0) > 0$), there is a sub-region (green) where the brightness decreases ($\Delta B_{n_{\mathrm{dmax}}}(d_0) < -5$ dB) with positive strain. These sub-regions are surrounded by the sub-region (gray) with low correlation ($R_{n_{\mathrm{dmax}}}(d_0) < 0.7$).

For regions $\mathbf{R_1}$ in Fig. 4(1), $\mathbf{R_3}$ in Fig. 4(3), and $\mathbf{R_4}$ in Fig. 4(4), the sub-region (yellow in Fig. 4(1-c), (3-c), and (4-c)) with high correlation and $\left|\Delta B_{n_{\mathrm{dmax}}}(d_0)\right| < 5$ dB but positive strain at the center was surrounded by the sub-region (blue) where the brightness increased ($\Delta B_{n_{\mathrm{dmax}}}(d_0) > 5$ dB), which was classified into Pattern I. For regions $\mathbf{R_2}$ in Fig. 4(2) and $\mathbf{R_5}$ in Fig. 4(5), inside the sub-region (yellow in Fig. 4(2-c) and (5-c)) with high correlation and $\left|\Delta B_{n_{\mathrm{dmax}}}(d_0)\right| < 5$ dB but positive strain, there is a sub-region (red) where the brightness increased ($\Delta B_{n_{\mathrm{dmax}}}(d_0) > 5$ dB), and these regions were classified into Pattern **II**.

Similarly, for Fig. 5, regions $\mathbf{R_6}$ in Fig. 5(1) and $\mathbf{R_9}$ in Fig. 5(4) were classified as Pattern I, and regions $\mathbf{R_7}$ in Fig. 5(2) and $\mathbf{R_8}$ in Fig. 5(3) were classified as Pattern II. In Fig. 6, region $\mathbf{R_{14}}$ in Fig. 6(5) was classified into Pattern I, region $\mathbf{R_{13}}$ in Fig. 6(4) was classified as Pattern II, and regions $\mathbf{R_{10}}$ in Fig. 6(1), $\mathbf{R_{11}}$ in Fig. 6(2), and $\mathbf{R_{12}}$ in Fig. 6(3) were classified as Pattern **III**. Thus, 16 regions with high correlation values ($R_{n_{\mathrm{dmax}}}(d_0) \geqq 0.7$) and $\left|\Delta B_{n_{\mathrm{dmax}}}(d_0)\right| < 5$ dB but positive strains ($\varepsilon(d_0) > 0$) analyzed in Figs. 5, 6, and 7 were roughly classified into one of the three patterns using $R_{n_{\mathrm{dmax}}}(d_0)$ and $\Delta B_{n_{\mathrm{dmax}}}(d_0)$.

Therefore, it is possible to roughly evaluate whether the measured strain $\varepsilon(d_0)$ is appropriate for estimating the elastic modulus. For plaque, not only the region where the correlation $R_{n_{\mathrm{dmax}}}(d_0)$ between the RF signals is low but also the region classified into one of the Patterns **I**, **II**, and **III** are unsuitable for estimation of the elastic modulus even when the correlation value $R_{n_{\mathrm{dmax}}}(d_0)$ is high and brightness does not change; i.e., the RF signal maintains its waveform and amplitude during one cardiac cycle.

Conclusion

In this study, the local changes in waveforms of RF signals and brightness inside the plaque caused by vessel dilatation were thoroughly observed to identify the targets where the strain measurement is unreliable for obtaining the elastic modulus of the plaque. For the healthy CCA, the change in the RF signals was small, and the strain $\varepsilon(d_0)$ was negative for all lateral positions. In contrast, for the plaque of the patient, there were some targets with large local changes in the RF signals. In these targets, the obtained strain $\varepsilon(d_0)$ was positive, which indicated that the calculation of the elastic modulus $E_\theta(d_0)$ was not suitable.

Furthermore, there were some regions where the change in RF signals was sufficiently small but the strain $\varepsilon(d_0)$ was positive. These regions were classified into one of three specific patterns characterized by the correlation $R_{n_{\mathrm{dmax}}}(d_0)$ and the brightness change $\Delta B_{n_{\mathrm{dmax}}}(d_0)$, as illustrated in Fig. 7. Thus, not only targets with a low correlation $R_{n_{\mathrm{dmax}}}(d_0)$ where the RF signals largely changed in waveform with vessel dilatation but also targets that were classified into one of the specific patterns were unsuitable for estimating the elastic modulus $E_\theta(d_0)$, even though the correlation $R_{n_{\mathrm{dmax}}}(d_0)$ was high during vessel dilatation.

As a preliminary study, this study provides a clue to assert the reliability of elasticity estimation inside plaque. Further research on the increase in the number of patterns by applying the method to many plaques from patients is necessary to ascertain the reliability more accurately. Another future study can consider elucidating the causes of these specific patterns of brightness change in the region where the correlation between the RF signals is high but the strain is positive.

Appendix: Derivation of the local elasticity of the arterial wall and the assumptions in Eq. (4)

In the estimation of the local elastic modulus $E_\theta(d_0)$, it is assumed that the vessel wall is elastically incompressible (Poisson ratio $\nu = 0.5$) and isotropic; the strain of the vessel wall in the axial direction, ε_z, can be negligible ($\varepsilon_z = 0$)

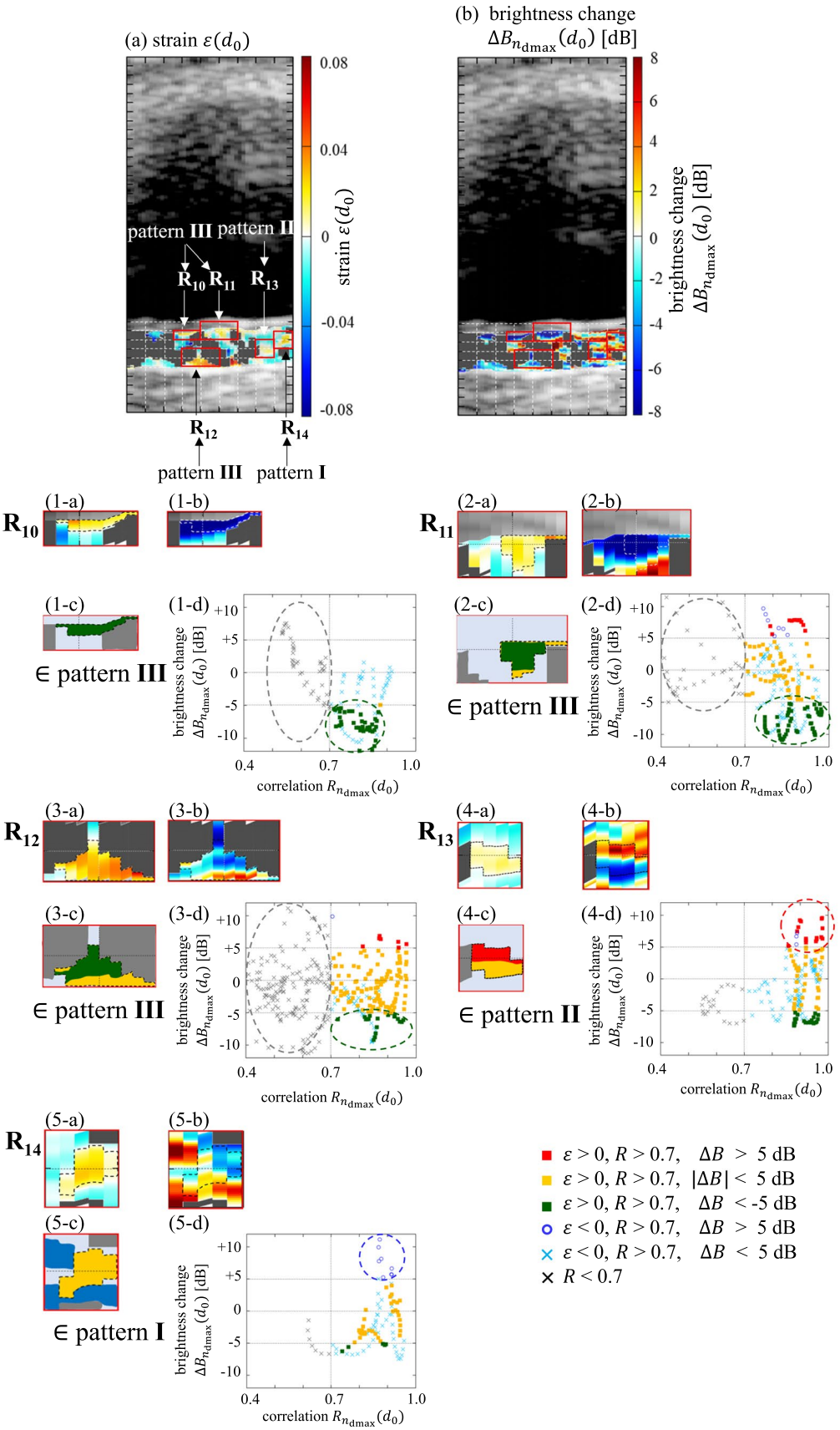

Fig. 6 For the third data from the carotid sinus of the same subject, **a**, **b** (**1**)–(**5**) are shown in a format similar to Fig. 4. In **a** and **b**, five regions $\mathbf{R_{10}}$–$\mathbf{R_{14}}$ where strains $\varepsilon(d_0)$ are positive are denoted by the red frames

because the artery is strongly restricted in the axial direction in vivo; and the change of inner radius Δr and the change of target thickness Δh_d are sufficiently small compared to the initial radius r_0 and the target thickness w at the time of R-wave, respectively. It is also assumed that the pressure in the vessel wall changes linearly from the pressure on the inner surface of the vessel wall (i.e., internal pressure of lumen) to the pressure outside the vessel (i.e., atmospheric pressure).

From the assumption of elastic isotropy, the local elastic modulus $E_\theta(d_0)$ in the circumferential direction on the local target set around the center depth d_0 with width w along the ultrasonic beam inside the wall is defined as [30]

$$E_\theta(d_0) = \left(\Delta\sigma_r(d_0) - \nu\Delta\sigma_\theta(d_0) - \nu\Delta\sigma_z(d_0)\right)\frac{1}{\varepsilon(d_0)}.[\mathrm{Pa}] \tag{A1}$$

The first term $\Delta\sigma_r(d_0)$ in Eq. (A1) is the time change of stress in the radial direction at a depth d_0. The second and third terms are the contribution of time changes of stresses $\Delta\sigma_\theta(d_0)$ in the circumferential direction and $\Delta\sigma_z(d_0)$ in the axial direction to the radial strain $\varepsilon(d_0)$ at depth d_0.

The radial stress $\sigma_r(d_0)$ is obtained by the average of stresses on the lumen and adventitia sides of the target. Under the assumptions mentioned above, $\Delta\sigma_r(d_0)$ is obtained as [31]

$$\Delta\sigma_r(d_0) = -\frac{1}{2}\left\{\Delta p'\left(d_0 - \frac{w}{2}\right) + \Delta p'\left(d_0 + \frac{w}{2}\right)\right\}, [\mathrm{Pa}] \tag{A2}$$

where $h_0 \geq w$ is the initial thickness of the vessel wall at the time of R-wave and $\Delta p'(d)$ is the time change of the pressure on depth d inside the wall. Under the assumption of linearity of pressure change in the wall [31], $\Delta p'(d)$ can be expressed using the pulse pressure Δp (time change of internal pressure of lumen minus atmospheric pressure) measured by a sphygmomanometer as

$$\Delta p'(d) = \frac{h_0 - (d - d_w)}{h_0}\Delta p.[\mathrm{Pa}] \tag{A3}$$

From the conditions for the equilibrium of forces in the radial direction on the target and the assumptions mentioned above, $\Delta\sigma_\theta(d_0)$ is obtained as [31]

$$\begin{aligned}\Delta\sigma_\theta(d_0) = {} & \frac{1}{w}\left(r_0 + d_0 - \frac{w}{2} - d_w\right)\Delta p'\left(d_0 - \frac{w}{2}\right) \\ & -\frac{1}{w}\left(r_0 + d_0 + \frac{w}{2} - d_w\right)\Delta p'\left(d_0 + \frac{w}{2}\right), [\mathrm{Pa}]\end{aligned} \tag{A4}$$

where $d_w < d_0$ is the depth of the interface between the lumen and the inner surface of the vessel wall at the time of R-wave. The first and second terms of Eq. (A4) are the contributions of pressures on the lumen side surface and the adventitia side surface of the target, respectively. $\Delta\sigma_z(d_0)$ is obtained from the assumption of $\varepsilon_z = 0$ as [30]

$$\Delta\sigma_z(d_0) = \nu\left(\Delta\sigma_r(d_0) + \Delta\sigma_\theta(d_0)\right).[\mathrm{Pa}] \tag{A5}$$

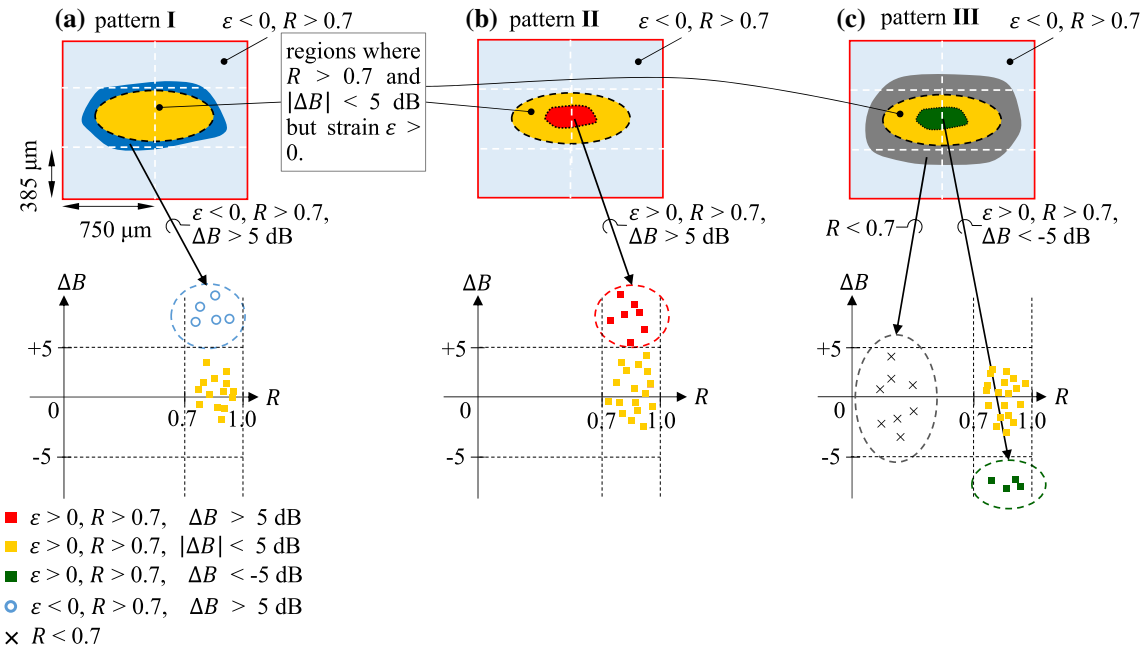

Fig. 7 **a** Pattern I, **b** pattern II, and **c** pattern III for explaining the sub-regions (yellow) with positive strain $\varepsilon(d_0)$ and high correlation ($R_{n_{\mathrm{dmax}}}(d_0) \geqq 0.7$) and the typical surroundings

By substituting Eqs. (A2, A3, A4, A5) into Eq. (A1), the local elastic modulus $E_\theta(d_0)$ on the target is obtained as

$$E_\theta(d_0) = \left\{\left(1-\nu^2\right)\Delta\sigma_r(d_0) - \nu(1+\nu)\Delta\sigma_\theta(d_0)\right\}\frac{1}{\varepsilon(d_0)}$$
$$= \frac{3}{4}\left(-\Delta\sigma_r(d_0) + \Delta\sigma_\theta(d_0)\right)\frac{1}{-\varepsilon(d_0)}$$
$$= \frac{3}{4}\left(\frac{1}{2} + \frac{r_0 + d_0 - \frac{w}{2} - d_w}{w}\right)\frac{\frac{w}{h_0}\Delta p}{-\varepsilon(d_0)}.[\mathrm{Pa}] \quad \text{(A6)}$$

Equation (A6) is the expansion of the elasticity definition derived by Hasegawa et al. [30] and equals the elasticity for the entire wall [30] by substituting $d_0 = d_w + h_0/2$ and $w = h_0$ into Eq. (A6). Thus, Eq. (4) is derived.

Acknowledgements The present work was supported in part by the Japan Society for the Promotion of Science KAKENHI Grants 20H02156 and 19KK0100.

Declarations

Conflict of interest The authors declare that they have no competing interests.

Ethical statement All the procedures followed were performed under the ethical standards of the responsible committee on human experimentation (institutional) and with the Helsinki Declaration of 1964 and later versions.

References

1. Fuster V, Badimon L, Badimon JJ, et al. The pathogenesis of coronary artery disease and the acute coronary syndromes. N Engl J Med. 1992;326:242–50.
2. Falk E. Why do plaques rupture? Circulation. 1992;86:30–42.
3. Shinohara M, Yamashita T, Tawa H, et al. Atherosclerotic plaque imaging using phase-contrast X-ray computed tomography. Am J Physiol Heart Circ Physiol. 2008;294:H1094–100.
4. Ravalli S, LiMandri G, Tullio MRD, et al. Intravascular ultrasound imaging of human cerebral arteries. J Neuroimaging. 1996;6:71–5.
5. Wada T, Takayama K, Myouchin K, et al. Usefulness of plaque diagnosis using intravascular ultrasound during carotid artery stenting. J Neuroendovascular Therapy. 2018;12:603–8.
6. Polak JF, Pencina MJ, Meisner A, et al. Associations of carotid artery intima-media thickness (IMT) with risk factors and prevalent cardiovascular disease. J Ultrasound Med. 2010;29:1759–68.
7. Duprez DA, De Buyzere ML, De Backer TL, et al. Relationship between arterial elasticity indices and carotid artery intima-media thickness. Am J Hypertens. 2000;13:1226–32.
8. Syeda B, Gottsauner-Wolf M, Denk S, et al. Arterial compliance: a diagnostic marker for atherosclerotic plaque burden? Am J Hypertens. 2003;16:356–62.
9. Bramwell JC, Hill AV. The velocity of the pulse wave in man. Proc R Soc Lond B Biol Sci. 1922;93:298–306.
10. Kim HL, Kim SH. Pulse wave velocity in atherosclerosis. Front Cardiovasc Med. 2019;6:1–13.
11. Hirai T, Sasayama S, Kawasaki T, et al. Stiffness of systemic arteries in patients with myocardial infarction. A noninvasive method to predict severity of coronary atherosclerosis. Circulation. 1989;80:78–86.
12. Ichino N, Osakabe K, Sugimoto K, et al. The stiffness parameter β assessed by an ultrasonic phase-locked echo-tracking system is associated with plaque formation in the common carotid artery. J Med Ultrason. 2012;39:3–9.
13. Selzer RH, Mack WJ, Lee PL, et al. Improved common carotid elasticity and intima-media thickness measurements from computer analysis of sequential ultrasound frames. Atherosclerosis. 2001;154:185–93.
14. Hasegawa H, Kanai H, Hoshimiya N, et al. Accuracy evaluation in the measurement of a small change in the thickness of arterial walls and the measurement of elasticity of the human carotid artery. Jpn J Appl Phys. 1998;37:3101–5.
15. Kanai H, Hasegawa H, Ichiki M, et al. Elasticity imaging of atheroma with transcutaneous ultrasound -preliminary study-. Circulation. 2003;107:3018–21.
16. Hasegawa H, Kanai H, Koiwa Y, et al. Measurement of change in wall thickness of cylindrical shell due to cyclic remote actuation for assessment of viscoelasticity of arterial wall. Jpn J Appl Phys. 2003;42:3255–61.
17. Inagaki J, Hasegawa H, Kanai H, et al. Construction of reference data for tissue characterization of arterial wall based on elasticity images. Jpn J Appl Phys. 2005;44:4593–7.
18. Inagaki J, Hasegawa H, Kanai H, et al. Tissue classification of arterial wall based on elasticity image. Jpn J Appl Phys. 2006;45:4732–5.
19. Tsuzuki K, Hasegawa H, Kanai H, et al. Threshold setting for likelihood function for elasticity-based tissue classification of arterial walls by evaluating variance in measurement of radial strain. Jpn J Appl Phys. 2008;47:4180–7.
20. Tsuzuki K, Hasegawa H, Ichiki M, et al. Optimal region-of-interest settings for tissue characterization based on ultrasonic elasticity imaging. Ultrasound Med Biol. 2008;34:573–85.
21. Yamagishi T, Kato M, Koiwa Y, et al. Usefulness of measurement of carotid arterial wall elasticity distribution in detection of early-stage atherosclerotic lesions caused by cigarette smoking. J Med Ultrason. 2006;33:203–10.
22. Yamagishi T, Kato M, Koiwa Y, et al. Evaluation of plaque stabilization by fluvastatin with carotid intima-medial elasticity measured by a transcutaneous ultrasonic-based tissue characterization system. J Atheroscler Thromb. 2009;16:662–73.
23. Yamagishi T, Kato M, Koiwa Y, et al. Impact of lifestyle-related diseases on carotid arterial wall elasticity as evaluated by an ultrasonic phased-tracking method in Japanese subjects. J Atheroscler Thromb. 2009;16:782–91.
24. Tokita A, Ishigaki Y, Okimoto H, et al. Carotid arterial elasticity is a sensitive atherosclerosis value reflecting visceral fat accumulation in obese subjects. Atherosclerosis. 2009;206:168–72.
25. Okimoto H, Ishigaki Y, Koiwa Y, et al. "A novel method for evaluating human carotid artery elasticity: Possible detection of early stage atherosclerosis in subjects with type 2 diabetes. Atherosclerosis. 2008;196:391–7.
26. Miyamoto M, Kotani K, Okada K, et al. Arterial wall elasticity measured using the phased tracking method and atherosclerotic risk factors in patients with type 2 diabetes. J Atheroscler Thromb. 2013;20:678–87.
27. Kaneko R, Sawada S, Tokita A, et al. Serum cystatin C level is associated with carotid arterial wall elasticity in subjects with type 2 diabetes mellitus: a potential marker of early-stage atherosclerosis. Diabetes Res Clin Pract. 2018;139:43–51.
28. Kume S, Hama S, Yamane K, et al. Vulnerable carotid arterial plaque causing repeated ischemic stroke can be detected with B-mode ultrasonography as a mobile component: Jellyfish sign. Neurosurg Rev. 2010;33:419–30.
29. Kanai H, Sato M, Koiwa Y, et al. Transcutaneous measurement and spectrum analysis of heart wall vibrations. IEEE Trans Ultrason Ferroelectr Freq Control. 1996;43:791–810.

30. Hasegawa H, Kanai H (2007) Strain imaging of arterial wall with translational motion compensation and error correction. In: Proceedings of 2007 IEEE International Ultrasonics Symposium, pp 860–3
31. Hasegawa H, Kanai H, Hoshimiya N, et al. Evaluating the regional elastic modulus of a cylindrical shell with nonuniform wall thickness. J Med Ultrason. 2004;31:81–90.
32. Céspedes I, Huang Y, Ophir J, et al. Methods for estimation of subsample time delays of digitized echo signals. Ultrason Imag. 1995;17:142–71.
33. Golemati S, Sassano A, Lever MJ, et al. Carotid artery wall motion estimated from B-mode ultrasound using region tracking and block matching. Ultrasound Med Biol. 2003;29:387–99.
34. Kitamura K, Hasegawa H, Kanai H. Accurate estimation of carotid luminal surface roughness using ultrasonic radio-frequency echo. Jpn J Appl Phys. 2012;51:07GF08-1–12.